Electron spectroscopy of Na-like autoionizing metastable ions

M. Lu and R. A. Phaneuf*
Department of Physics, MS 220, University of Nevada, Reno, Nevada 89557-0058
(Received 20 December 2001; published 19 July 2002)

Ejected electrons from the decay of metastable $2p^5 3s3p\ ^4D_{7/2}$ autoionizing states of Na-like Ar^{7+}, Cl^{6+}, and S^{5+} have been detected using an ion-beam delayed-coincidence technique. The previously calculated and measured Ar^{7+} Auger line at 114.10 ± 0.33 eV was used to calibrate a high-efficiency two-stage parallel-plate electron spectrometer. The energies of the corresponding Auger lines from decay of metastable Cl^{6+} and S^{5+} were subsequently determined to be 102.0 ± 1.2 eV and 86.6 ± 1.0 eV, respectively. The results are consistent with published data for other members of the Na isoelectronic sequence, and they together exhibit a quadratic scaling with ionic charge q over the range $4 \leqslant q \leqslant 15$.

DOI: 10.1103/PhysRevA.66.012706 PACS number(s): 32.80.Dz

I. INTRODUCTION

The properties of highly stripped, excited atoms are of both fundamental and practical interest. Excited ions play important roles in the diagnostics of laboratory and astrophysical plasmas [1]. Metastable ionic states have also been considered in the design of short-wavelength lasers [2]. In many cases the quartet level of highest J of a given configuration of an alkali atom or ion is metastable against autoionization, so that the branching ratio for radiation in the extreme ultraviolet (XUV) is appreciable. Such states are therefore candidates for the upper level of XUV lasers, or may provide intermediate levels for store and transfer lasers [3]. The core-excited states of Na-like ions, which have two outer M-shell electrons and a single vacancy in an otherwise filled L shell, are of particular interest. Two outer electrons are required because the lower laser level is then a closed-shell system with one outer electron. The lower-level population may be quenched by ionization of the remaining electron. Since the upper level can Auger decay, it is important to consider possible upper levels for which the Auger decay rate is smaller than or comparable to the radiative decay rate [4].

The $2p^5 3s3p\ ^4D_{7/2}$ metastable state, which has the highest J for this configuration, has been studied theoretically and experimentally for several Na-like ions. The energy of Auger electrons from this state of Fe^{15+} was measured and its metastable nature demonstrated by Schneider *et al.* [5] in an ion-atom collision experiment. Karim *et al.* [6] have performed detailed theoretical studies of x-ray wavelengths, Auger energies, and decay rates for P^{4+}. The autoionization spectrum of Ar^{7+} has been calculated by Chen [7] using the multiconfiguration Dirac-Fock method. The Auger electron energy and lifetime of this metastable state for Ar^{7+} were calculated to be 114.09 eV and 3.2 μs, respectively. Hutton *et al.* [8,9] measured this Auger line in ion-atom collision experiments at an energy of 114.10 ± 0.33 eV, in excellent agreement with the theoretical result. This Ar^{7+} line was therefore selected as a benchmark to calibrate the energy scale of a newly developed electron spectrometer.

In this paper, an electron-ion delayed-coincidence technique developed to measure ejected electron spectra due to electron-ion collisions is described. As an initial test of this apparatus, the energies of Auger electrons from the decay of the long-lived $2p^5 3s3p\ ^4D_{7/2}$ states of Na-like Cl^{6+} and S^{5+} were measured.

II. EXPERIMENTAL SETUP

The apparatus and coincidence technique described in this section were developed with an ultimate goal of measuring the energy distribution of electrons ejected in ionizing electron-ion collisions. The coincident measurement of electrons and ions from autoionization of a fast metastable Na-like ion beam reported here represent an initial proof-of-principle test of the method [10]. In the present experiment the metastable ions were created in the ion source plasma along with predominantly ground-state ions. Since the microsecond lifetimes of these metastable states are comparable to ion flight times in the experiment, the metastable ions constituted a small component of the ion beam that spontaneously autoionized along its flight path.

A. Ion beam

The experiments were performed at the Multicharged Ion Research Facility at the University of Nevada, Reno [11]. Multiply charged ions were produced in a 14.4-GHz Caprice two-stage electron-cyclotron resonance ion source [12]. Gas (Ar, CCl_4, or H_2S) was injected into the plasma chamber and ionized by successive collisions with energetic electrons. The ion beam was extracted from the ion source by a potential difference of 10 kV, and transmitted by an ion-beam transport system consisting of two einzel lenses and two sets of steering plates. The desired ion beam is selected according to momentum/charge by a double-focusing dipole analyzing magnet. The beam size and analyzer resolution are determined by adjustable four-jaw slits located downstream at the focus of the analyzing magnet. Another einzel lens and set of steering plates behind the analyzing magnet direct the ion beam to the experiments that are located downstream. The operating pressure in the ion source plasma discharge chamber was approximately 10^{-6} Torr, and was typically 10^{-9}

*Electronic address: phaneuf@physics.unr.edu

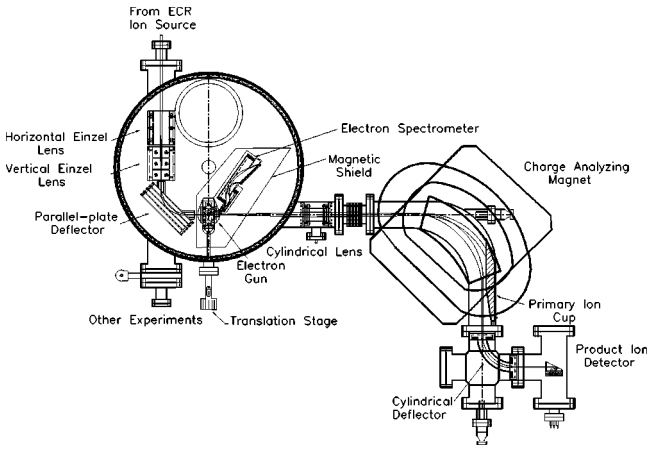

FIG. 1. Schematic of crossed-beams coincidence apparatus.

Torr in the ion-beam transport system. The collimated ion-beam currents for this experiment were 250 nA for $^{40}Ar^{7+}$, 25 nA for $^{35}Cl^{6+}$, and 12 nA for $^{32}S^{5+}$.

B. Crossed-beam apparatus

A schematic diagram of the crossed-beam apparatus developed for absolute measurement of electron-impact ionization cross sections [13] is presented in Fig. 1. The ion beam is focused and positioned by independent one-dimensional einzel lenses and steering elements, and directed to the interaction region by a 90° parallel-plate analyzer, which removes ions from the beam that have changed charge in transport. The interaction region, which is enclosed by a magnetic shield, contains an electron gun and an electron spectrometer. The electron gun was not activated for the measurements reported here. Electrons emitted by the ion beam enter the electron spectrometer at 15° with respect to the ion-beam axis, and are analyzed and detected by a two-stage 30° parallel-plate electron spectrometer. The ion beam (which also contains further ionized products) is focused downstream of the interaction region by a cylindrical einzel lens and analyzed by a 90° dipole charge-analyzing magnet. The product ions are magnetically deflected by 90°, while the primary ions of lower charge are deflected through a smaller angle (depending on the final-to-initial charge ratio) and collected by an extended Faraday cup mounted inside the magnet chamber. The product ions are further dispersed by a 90° cylindrical electrostatic analyzer and directed to a stainless-steel plate biased at -400 V, from which secondary electrons are detected by a pair of microchannel plates (MCP) operated in single-particle counting mode.

C. Electron spectrometer

A two-stage 30° parallel-plate electron spectrometer with a position-sensitive electron detector was developed for the present application. Due to second-order focusing, this instrument has a higher efficiency and resolution than other commonly used designs [14]. The spectrometer, shown in Fig. 2, is similar to that developed by Swenson for ion-atom collision experiments [15]. A position-sensitive electron detector consisting of a custom tandem microchannel-plate detector with an active area of 15 mm$\times$100 mm and a resistive-anode encoder (RAE) provides an effective energy bandwidth $2(E_{min}-E_{max})/(E_{min}+E_{max})$ of 48%. The entrance aperture is 0.37 cm high$\times$0.185 cm wide, giving a solid angle of acceptance in the present application of 0.046 sr and an energy resolution of 5%. High-transmission (95%) grids on the high-voltage plates of both stages backed by grounded shields serve to suppress the emission of secondary electrons produced by high-energy electrons and photons. Resistive dividers provided the appropriate voltages to the two stages of the spectrometer, and to ''picture-frame'' electrodes that assured uniformity of the electric fields. The performance of the spectrometer was modeled using analytical solutions [14] as well as the SIMION 3D charged-particle trajectory computer code [16].

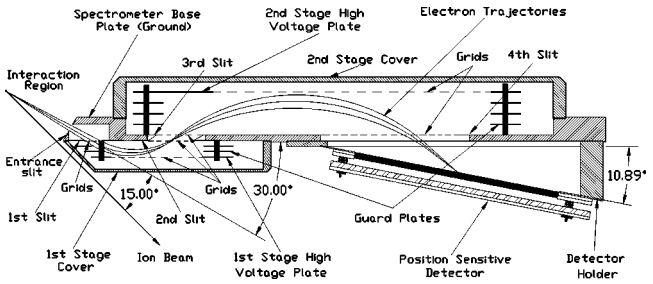

FIG. 2. Schematic of two-stage 30° parallel-plate electron spectrometer. In the crossed-beams arrangement, the electron-beam axis is perpendicular to the page and located at the center of the interaction region.

D. Electron-ion coincidence technique

Acquiring an ejected electron energy spectrum due to electron-impact ionization of an ion in a crossed-beams experiment requires detection of an electron signal in the proximity of an electron beam of 10^{12}–10^{15} times higher intensity. An electron-ion delayed-coincidence technique was implemented to address this requirement. Ion flight times from the interaction region to the ion detector were in the 3–4 μs range. Fast timing signals for the delayed-coincidence measurement were obtained from the rear surface of the second MCP of the chevron electron detector and from the product ion MCP detector. The time difference between these signals was recorded by a time-to-digital converter with a resolution of 7.8 ns/channel. Two charge signals extracted from opposite ends of the RAE of the electron detector provide a one-dimensional position (and therefore energy) spectrum. The latter was obtained by directing the two amplified and shaped charge signals from the RAE to analog-to-digital converters. Each detected electron was therefore characterized by both its position of impact on the detector face and by the time elapsed until the subsequent detection of an ion whose charge had increased by one unit.

III. EXPERIMENTAL RESULTS

A. Electron spectrometer calibration

Energy calibration of the electron spectrometer was carried out using the known Auger line (114.10 eV) from the

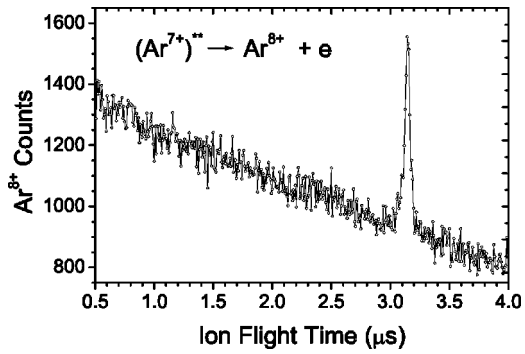

FIG. 3. Time-of-flight spectrum for 70 keV Ar^{8+} due to autoionization of metastable Ar^{7+}. The peak at 3.14 μs corresponds to an Ar^{8+} ion flight path of 182 cm from the interaction region to the ion detector. The time resolution of the time-to-digital converter is 7.8 ns/channel.

decay of the $2p^5 3s3p\ ^4D_{7/2}$ metastable state of Ar^{7+}. The count rate in the product ion detector was typically 500 s^{-1} $nA^{-1}$and the true coincidence rate was 0.002 s^{-1} $channel^{-1}$ for a typical Ar^{7+} ion-beam current of 250 nA (electrical). Several days of continuous data acquisition were required to obtain acceptable statistical precision in a single measurement. Figure 3 presents a typical time-of-flight spectrum, taken with a temporal resolution of 7.8 ns/channel. Figure 4 presents measurements of the coincident position spectrum corresponding to a time delay in the product ion channel of 3.14 μs. The energy scale of the

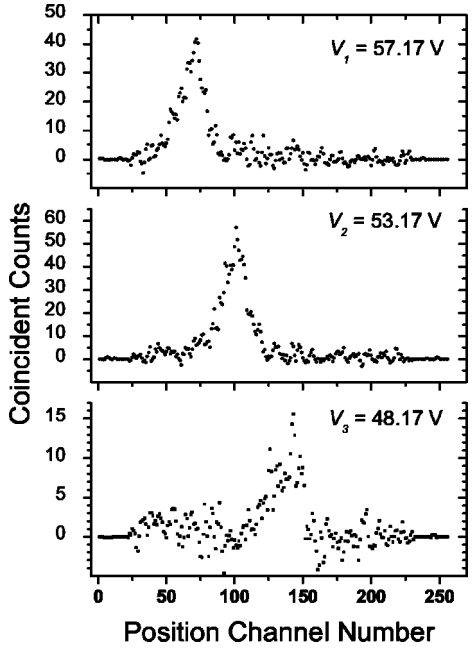

FIG. 4. Electron detector position spectra due to autoionization of metastable 70 keV Ar^{7+} coincident with an ion flight time of 3.14 μs at three different voltages V_i applied to the electron spectrometer. The feature corresponds to an electron ejected with an energy of 114.10 eV in the center-of-mass frame, which corresponds to 135.10 eV in the laboratory frame. A noncoincident background has been subtracted from each spectrum.

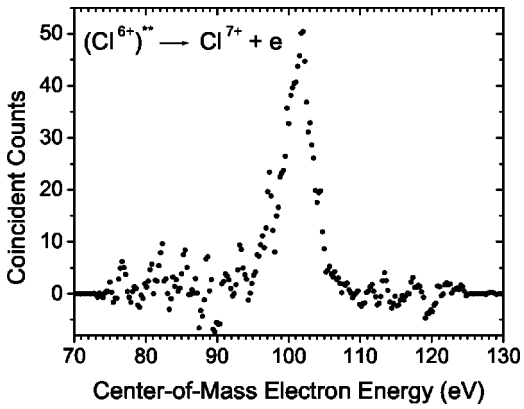

FIG. 5. Coincidence electron energy spectrum due to autoionization of metastable Cl^{6+}. Voltage $V_i = 44.10$ V was applied to the electron spectrometer. A noncoincident background has been subtracted from the spectrum.

spectrometer was calibrated by accumulating coincidence spectra for different values of the voltage V_i applied to the spectrometer, as shown, and by using the following equations:

$$E_{min} = A_1 V_i , \tag{3.1}$$

$$E = E_{min} + A_2 C_i V_i = A_1 V_i + A_2 C_i V_i , \tag{3.2}$$

where E_{min} is the minimum detectable electron energy, E is the electron energy in the laboratory frame, V_i is the voltage applied to the first-stage high-voltage plate of the electron spectrometer ($0.92V_i$ is applied to the second-stage high-voltage plate), and C_i is the channel number, corresponding to the horizontal position at which an electron impacts the detector (maximum of 256). A_1 and A_2 are calibration coefficients that may be estimated from the modeling but must be determined experimentally for accurate measurements. A_1 and A_2 and their uncertainties were obtained by accumulating coincidence spectra with three different voltages V_i applied to the electron spectrometer, and recording the corresponding central channel number C_i for the Auger line. The

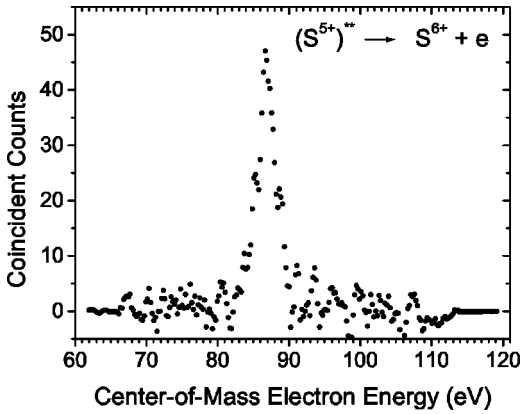

FIG. 6. Coincidence electron energy spectrum due to autoionization of metastable S^{5+}. Voltage $V_i = 40.04$ V was applied to the electron spectrometer. A noncoincident background has been subtracted from the spectrum.

TABLE I. Measured Auger electron energies for decay of $2p^5 3s3p\ ^4D_{7/2}$ metastable Na-like ions.

Ion	Energy(eV)
Ar^{7+}	114.10 ± 0.33[a]
Cl^{6+}	102.0 ± 1.2
S^{5+}	86.6 ± 1.0

[a]Reference value [7–9] for spectrometer energy calibration.

following results were obtained: $A_1 = 1.922 \pm 0.015$, $A_2 = (6.130 \pm 0.015) \times 10^{-3}$. These values are within 10% of those predicted by SIMION 3D modeling.

B. Coincident electron spectroscopy of metastable Cl^{6+} and S^{5+} ions

Subsequent to calibration of the electron spectrometer, corresponding coincidence measurements were made with beams of 60 keV $^{35}Cl^{6+}$ and 50 keV $^{32}S^{5+}$. The product ion count rates were larger than for Ar^{7+}: 3000 s^{-1} nA^{-1} for Cl^{6+} and 14 000 s^{-1} nA^{-1} for S^{5+}. The delayed coincidence rates were comparable to the Ar^{7+} case: 0.002 s^{-1} $channel^{-1}$ for $^{35}Cl^{6+}$ and 0.003 s^{-1} $channel^{-1}$ for $^{32}S^{5+}$, requiring data acquisition times of 65 and 61 h, respectively, to achieve acceptable statistical precision in the electron energy spectrum. The results are presented in Fig. 5 and Fig. 6, and are compared to the Ar^{7+} calibration data in Table I. It is instructive to compare the present data to published data for other Na-like ions. The scaling of the measured and calculated electron energies with ionic charge for the five members of the Na isoelectronic sequence is presented in Fig. 7. The curve represents a quadratic fit to the data, represented by the equation:

$$E = 28.768 + 9.958\,q + 0.337\,q^2, \tag{3.3}$$

where q is the ionic charge. The present measurements for Cl^{6+} and S^{5+} are consistent with published experimental and theoretical data for the Na isoelectronic sequence, and the quadratic scaling of electron energies with ionic charge fits the data in the range $4 \leqslant q \leqslant 15$ with a mean deviation of ± 0.66 eV.

IV. SUMMARY AND OUTLOOK

Measurement of the energy of electrons ejected from a fast autoionizing metastable ion beam has been demonstrated using an electron-ion delayed-coincidence technique. The method has been used with a metastable Ar^{7+} beam to calibrate a two-stage parallel-plate electron spectrometer with an energy bandpass of 48% and a resolution of 5%. The technique has been applied to the first measurements of the energy of electrons from the autoionization of $2p^5 3s3p\ ^4D_{7/2}$ metastable Na-like Cl^{6+} and Cl^{5+}. The measured energies are consistent with existing experimental and theoretical data for other Na-like ions, and help to establish a scaling along the isoelectronic sequence.

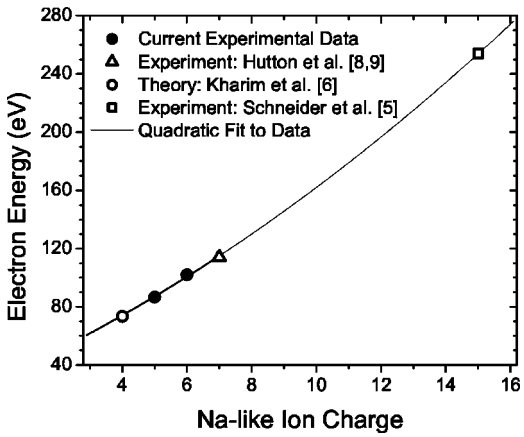

FIG. 7. Scaling of measured and calculated electron energies from autoionization of $2p^5 3s3p^4D_{7/2}$ metastable Na-like Fe^{15+}, Ar^{7+}, Cl^{6+}, and S^{5+} and P^{4+} with ionic charge. The curve represents a quadratic fit to the data.

This technique will next be applied to measurement of the energy spectrum of ejected electrons produced in electron-ion collisions. The product ion background count rate will be significantly lower for such measurements, due to the absence of metastable autoionizing states in the parent ion beam. However, this will be more than offset by a significant increase in the background count rate in the electron spectrometer, since it must be aimed directly at the crossing of the ion beam with an electron beam carrying a current in the microampere range. The challenge will be to reduce that count rate to an acceptable level while maintaining sufficient electron-beam current to yield a measurable electron-ion signal and coincident count rate.

ACKNOWLEDGMENTS

The authors are grateful to J. K. Swenson for the design of the electron spectrometer, to D. Meredith for its skillful construction, to R. Rejoub for preliminary modeling calculations, and to A. Müller for helpful comments on the manuscript. Special thanks are owed to R. M. Ali and A. A. Hasan for invaluable assistance with the implementation of the position-sensitive detector and coincidence data acquisition system. This research was supported by the Division of Chemical Sciences, Biosciences and Geosciences of the US Department of Energy under Contract No. DE-FG03-00ER14787 with the University of Nevada, Reno.

[1] Hans R. Griem, *Principles of Plasma Spectroscopy*, Cambridge Monographs on Plasma Physics (Cambridge University Press, New York, 1997), Vol. 2.

[2] J. E. Rothenberg and S. E. Harris, IEEE J. Quantum Electron. **QE-17**, 418 (1981).

[3] S. E. Harris, D. J. Walker, R. G. Caro, A. J. Mendelsohn, and

R. D. Cowan, Opt. Lett. **9**, 168 (1984).
[4] E. J. McGuire, Phys. Rev. A **14**, 1402 (1976).
[5] D. Schneider, M. H. Chen, S. Chantrenne, R. Hutton, and M. H. Prior, Phys. Rev. A **40**, 4313 (1989).
[6] Kh Rezaul Karim, Mau Hsiung Chen, and Bernd Crasemann, Phys. Rev. A **28**, 3355 (1983).
[7] Mau Hsiung Chen, Phys. Rev. A **40**, 2365 (1989).
[8] R. Hutton, M. H. Prior, S. Chantrenne, Mau Hsiung Chen, and D. Schneider, Phys. Rev. A **39**, 4902 (1989).
[9] R. Hutton, D. Schneider, and M. H. Prior, Phys. Rev. A **44**, 243 (1991).
[10] M. Lu, M.S. thesis, University of Nevada, Reno (2001).
[11] R. A. Phaneuf *et al.*, in *Applications of Accelerators in Research and Industry*, edited by J. L. Duggan and I. L. Morgan, AIP Conf. Proc. No. 392 (AIP, Woodbury, New York, 1997), pp. 89–92.
[12] D. Hitz, P. Ludwig, G. Melin, and M. Pontonnier, Nucl. Instrum. Methods Phys. Res. B **98**, 517 (1995).
[13] R. Rejoub and R. A. Phaneuf, Phys. Rev. A **61**, 032706 (2000).
[14] T. S. Green and G. A. Proca, Rev. Sci. Instrum. **41**, 1409 (1970).
[15] J. K. Swenson, Nucl. Instrum. Methods Phys. Res. B **10/11**, 899 (1985).
[16] D. A. Dahl, Idaho National Engineering and Environmental Laboratory Report INEEL-95/0403, 2000 (unpublished).